

Reinforcement Learning Goal-Reaching Control with Guaranteed Lyapunov-Like Stabilizer for Mobile Robots

Mehdi Heydari Shahna^{a,*}, Seyed Adel Alizadeh Kolagar^{a,*}, Jouni Mattila^a

^a*Faculty of Engineering and Natural Sciences, Tampere University, Tampere, 33720, Finland*

Abstract

Reinforcement learning (RL) can be highly effective at learning goal-reaching policies, but it typically does not provide formal guarantees that the goal will always be reached. Without formal guarantees, despite RL's potential to gain performance and autonomy, international standards limit their adoption in operational industries, where exploratory interactions with state action pairs can be hazardous, especially when operating in challenging environments. A common approach to provide formal goal-reaching guarantees is to introduce a shielding mechanism that restricts the agent to actions that satisfy predefined safety constraints. The main challenge here is integrating this mechanism with RL so that learning and exploration remain effective without becoming overly conservative. Hence, this paper proposes an RL-based control framework that provides formal goal-reaching guarantees for wheeled mobile robots operating in unstructured environments. To achieve this, we first design a real-time RL policy with a set of 15 carefully defined reward terms. These rewards encourage the robot to reach both static and dynamic goals while generating sufficiently smooth command signals that comply with predefined safety specifications, which is critical in practice. Second, a Lyapunov-like stabilizer layer is integrated into the benchmark RL framework as a policy supervisor to formally strengthen the goal-reaching control while preserving meaningful exploration of the state action space. The proposed framework is suitable for real-time deployment in challenging environments, as it provides a formal guarantee of convergence to the intended goal states and compensates for uncertainties by generating real-time control signals based on the current state, while respecting real-world motion constraints. The proposed control framework is validated on a 6,000 kg robot operating in a slip-prone terrain. The results show that the proposed Lyapunov-like stabilizer consistently improves the benchmark RL policies, boosting the goal-reaching rate from 84.6% to 99.0%, sharply reducing failures, and improving efficiency by lowering episode lengths and steps-to-goal while maintaining safe, conservative fallback behavior. Comparative results also showed high performance in the proposed strategy in terms of accuracy and control effort.

Keywords: Lyapunov stability; nonlinear control; reinforcement learning

1. Introduction

Reinforcement learning (RL) involves an agent repeatedly interacting with an environment to learn a control or decision policy that maximizes cumulative reward. It has shown strong performance across many domains, but key challenges remain, including reproducibility, convergence guarantees, and the large amounts of data and training iterations often required [1]. RL methods are commonly categorized as model-based or model-free. Model-based approaches use known or estimated system dynamics to compute a policy, whereas model-free approaches learn directly from experience without an explicit model, using methods such as value-function learning, policy gradients, and actor-critic algorithms [2]. In mobile robotics, model-free RL is particularly attractive when accurate dynamics are unavailable or prohibitively expensive to model. However, ensuring that learned policies are safe and satisfy state constraints during real-world operation remains a major challenge [3]. Hence,

international standards limit the adoption of RLs in many operational industries, where exploratory interactions with state action pairs can be hazardous, especially when operating in challenging environments [4]. For instance, it is rare to find studies that have deployed RL strategies on large-scale robots operating in challenging environments, such as off-road terrain, under significant uncertainty and disturbances, despite RL's potential to gain performance and autonomy [5].

Most safety-assured RL methods rely on Lyapunov and barrier certificates, including Control Lyapunov Functions (CLFs), Barrier Lyapunov Functions (BLFs), and Control Barrier Functions (CBFs), to guarantee closed-loop goal reaching and enforce safety constraints. These tools integrate naturally with RL because their conditions can be expressed as constraints involving learnable function approximators [2, 6]. In brief, a CLF is used to synthesize control inputs that drive the state toward a desired equilibrium, a BLF enforces state constraints by becoming unbounded at the constraint boundary so trajectories remain within the admissible set, and a CBF guarantees safety by imposing inequality constraints that render a specified safe set forward invariant. Several representative approaches follow

*These authors contributed equally to this paper and are co-first authors.

Corresponding author: Mehdi Heydari Shahna

E-mail address: mehdi.heydarishahna@tuni.fi

this paradigm. Emam et al. [7] combine RL with a robust CBF-based safety layer that solves a small optimization problem at each time step to minimally modify the policy action while ensuring safety, even under model uncertainty. Because the layer is differentiable, the policy can be trained through it, enabling safe exploration and improved learning in robotic tasks. Zhang et al. [8] embed BLFs within a backstepping actor-critic design, where the barrier function (BF) term grows rapidly near constraint limits, and Lyapunov analysis maintains boundedness, keeping trajectories within the safe set during learning under uncertainty. Jabari et al. [9] treat CBF and BLF approaches as safety baselines and propose a monotone tube boundary to enforce tracking-error constraints with less design complexity than CBFs and less conservatism than BLFs. They then use an actor-critic scheme to learn an approximately optimal prescribed-time controller that trades off tracking accuracy and control effort, with the added benefit of reducing power consumption and actuator heating. Chow et al. [10] cast safe RL as maximizing return subject to a constraint on cumulative safety cost (for example, reaching a goal while limiting collisions). They construct a Lyapunov function from a feasible baseline policy and restrict policy updates to remain within the Lyapunov-feasible set, so safety is maintained during both training and deployment. Zhao et al. [11] enforce stepwise CBF constraints to keep the state inside a forward-invariant safe set and add a Lyapunov decrease condition using a learned Lyapunov value function (Lyapunov network) to promote stability in control-affine Markov decision process (MDP) settings. When safety and stability cannot be simultaneously satisfied, a backup controller is used. Li et al. [12] build a CLF from reference tracking error and incorporate both the CLF value and its decay condition into the training reward, shaping learning toward faster convergence and improved robustness while reducing reliance on hand-tuned reward terms (used during training only). Similarly, Anand et al. [13] discuss CLF-based stability certification in RL, either by interpreting the value function as a Lyapunov function or by enforcing Lyapunov decrease conditions to estimate and expand a safe region of attraction, thereby keeping exploration and the learned policy stable and safe.

A key contribution of the mentioned CBFs and BLFs for RLs is that they can preserve safety guarantees based on barrier functions (BFs) throughout exploration while still allowing effective learning. This helps the resulting policy trade off constraint satisfaction with task success, although for general systems, constructing an appropriate BF is often a nontrivial, highly problem-dependent design task within RLs. CLF-based methods for RLs have also demonstrated strong results in both simulation and on small physical robots, supporting safe and efficient exploration in changing environments, but they generally assume a Lyapunov function is available in advance or other hand-crafted safety ingredients (or ad hoc formal derivations, post hoc verification, or extra assumptions that often restrict applicability). Moreover, there is no demonstrated deployment of these ideas on large, multi-ton robotic systems on a challenging environment, where uncertainty and disturbances are often much more severe and destructive.

To tackle the mentioned difficulties and apply a formal-

guaranteed goal-reaching RL policy on large robotic platforms in a slip-prone environment, this paper develops [14]. First, we design a vision-driven, smooth control scheme for goal-reaching that uses a real-time RL policy with a set of 15 carefully defined reward terms. These rewards encourage the robot to reach both static and dynamic goals while generating sufficiently smooth command signals that comply with predefined safety specifications, which is critical in practice to keep healthy connections with the visual-based pose estimation module. We then integrate the benchmark goal-reaching RL policy with a Lyapunov-like stabilizer agent to provide formal convergence guarantees to a target goal set, without requiring prior knowledge of the Lyapunov function. The key findings of this research are as follows. 1) In contrast to [15, 16, 17], we define the action space in terms of linear and angular accelerations rather than velocities to generate smooth motion commands and reduce discontinuities caused by pose-estimation updates, as it is intended for real-time use and to mitigate disturbances such as wheel slip, a frequent issue for outdoor vehicles. The jerks (derivative of accelerations), accelerations, and velocities are bounded according to the system specifications. 2) The proposed method is positioned as a practical alternative to guarantee-focused RL approaches that assume a known Lyapunov function, for example [13, 8], and to emergency safety mechanisms that simply halt the system when unsafe states are detected, as in [14] and [18]. 3) The proposed approach, in addition to solid theoretical proof, is supported by experiments on a 6000 kg large skid steer wheeled mobile robot (WMR). 4) In contrast to BF-based approaches that irrevocably exclude some state-action combinations, the proposed Lyapunov-like stabilizer does not make any combination inherently unreachable. Overall, this paper presents the first real-world RL-based goal-reaching control framework for a multi-ton robot operating in an off-road environment that provides formal guarantees without requiring prior knowledge of a Lyapunov function and without relying on overly conservative safety shields.

The remainder of this paper is organized as follows. In Section 2, the problem is formulated, and in Section 3, the proposed benchmark RL goal-reaching policy is developed subject to motion constraints. Next, in Sections 4 and 5, the proposed Lyapunov-like stabilizer is introduced to formally enhance the benchmark RL policy. Finally, Section 6 reports numerical and experimental validations of the complete framework on a 6000 kg WMR.

2. Problem Definition

Let us consider the MDP defined as follows [19]

$$\mathcal{M} = (\mathcal{S}, \mathcal{A}, \mathcal{P}, \mathcal{C}) \quad (1)$$

Let \mathcal{S} be a finite or countable set of discrete states, modeled as a finite-dimensional normed linear space, and let \mathcal{A} be the actions, taken as a compact subset of an appropriate topological space. The dynamics are specified by a stochastic kernel $\mathcal{P}(s_{t+1} | s_t, a_t)$ on \mathcal{S} , so after applying a given action a_t at the current state s_t , the successor s_{t+1} is distributed according to

$\mathcal{P}(\cdot | s_t, a_t)$. Immediate performance is quantified by a one-step cost map $C : \mathcal{S} \times \mathcal{A} \rightarrow \mathcal{R}$, with the immediate cost c_t . All randomness is defined on $(\Omega, \mathcal{F}, \mathcal{P})$, and expectations are taken via E . The RL task is to choose a policy $\pi \in \Pi$ that minimizes:

$$\begin{aligned} V^\pi(s) &= -E_\pi \left[\sum_{t=0}^{T_{\text{end}}} \gamma^t R_t | S_0 = s \right] \\ &= E_\pi \left[\sum_{t=0}^{T_{\text{end}}} \gamma^t c(S_t, A_t) | S_0 = s \right] \end{aligned} \quad (2)$$

where T_{end} denotes the stopping time, namely the step at which the goal is achieved, the episode times out, or the agent exits the permitted workspace. γ^t is the discount factor $\gamma \in [0, 1)$ at t , giving the weight applied to the stage cost/reward. R_t is the reward at t , typically defined as the negative of the stage cost. $s \in \mathcal{S}$ denotes a fixed initial state value, S_0 is the corresponding initial-state random variable with the conditioning $S_0 = s$, and S_t and A_t denote the (generally random) state and action at time step t generated by the policy π and the environment dynamics. Any policy π^* that achieves the best (minimum) objective value is called optimal. In this context, an agent is simply a finite algorithm that chooses actions based on the states it observes. This paper considers the design of a goal-reaching RL policy for WMRs that (i) guarantees formal goal-reaching and (ii) satisfies predefined motion specifications that enforce sufficiently smooth behavior. Motion smoothness is treated as a critical requirement because aggressive or non-smooth maneuvers can induce shocks and vibrations that degrade or interrupt vision-based pose estimation in real-world operation, thereby compromising closed-loop performance.

3. Benchmark Motion-Constrained RL Goal-Reaching Policy

In this work, the system's state at time t is represented by x_t, y_t, θ_t, v_t , and ω_t , where $P_t = (x_t, y_t) \in \mathbb{R}^2$ specifies the robot's location, θ_t its orientation, v_t its forward speed, and ω_t its rotational speed. For a target point $X_G = (x_g, y_g)$, we then define

$$\begin{aligned} d_t(P_t, X_G) &= \sqrt{(x_g - x_t)^2 + (y_g - y_t)^2}, \\ e_t &= \text{wrap}_\pi(\text{atan2}(y_g - y_t, x_g - x_t) - \theta_t) \end{aligned} \quad (3)$$

where d_t denotes the goal distance and e_t represents the orientation (heading) error. These variables are then quantized by partitioning them into discrete bins, as follows:

$$\begin{cases} \text{Distance } d^{(1)}, \dots, d^{(N_d)} \text{ over } [0, d_{\max}], \\ \text{Heading error } e^{(1)}, \dots, e^{(N_\theta)} \text{ over } [-\pi, \pi], \\ \text{Linear vel. } v^{(1)}, \dots, v^{(N_v)} \text{ over } [v^{\min}, v^{\max}], \\ \text{Angular vel. } \omega^{(1)}, \dots, \omega^{(N_\omega)} \text{ over } [\omega^{\min}, \omega^{\max}] \end{cases} \quad (4)$$

The discretized state is defined as $s_t = q(d_t, e_t, v_t, \omega_t) = (i_d, i_e, i_v, i_\omega)$, where each component index comes from quantizing $(d_t, e_t, v_t, \omega_t)$ into bins $q : \mathbb{R}^4 \rightarrow \mathcal{S}$, and the resulting 4D index tuple is mapped into a single integer label. In contrast to [20], the controller was designed to produce smoother

commands by having the agent select linear and angular accelerations, rather than commanding v and ω directly, so $a_t = (a_{v,t}, a_{\omega,t}) \in \mathcal{A}$. The action set \mathcal{A} is implemented as a finite grid, as follows:

$$\begin{cases} a_{v,t} \in \{a_v^{(1)}, \dots, a_v^{(N_{av})}\} \subset [a_v^{\min}, a_v^{\max}], \\ a_{\omega,t} \in \{a_\omega^{(1)}, \dots, a_\omega^{(N_{a\omega})}\} \subset [a_\omega^{\min}, a_\omega^{\max}] \end{cases} \quad (5)$$

and \mathcal{A} is formed as the Cartesian product of those component sets. For a given state and chosen action, the system evolves according to the following dynamics:

$$\begin{cases} v_{t+1} = \text{sat}(v_t + a_{v,t} \Delta t, v^{\min}, v^{\max}), \\ \omega_{t+1} = \text{sat}(\omega_t + a_{\omega,t} \Delta t, \omega^{\min}, \omega^{\max}), \\ x_{t+1} = x_t + v_{t+1} \cos(\theta_t) \Delta t, \\ y_{t+1} = y_t + v_{t+1} \sin(\theta_t) \Delta t, \\ \theta_{t+1} = \text{wrap}_\pi(\theta_t + \omega_{t+1} \Delta t), \end{cases} \quad (6)$$

where $\text{sat}(\cdot)$ denotes a saturation function and Δt is the sampling interval. The operating area is rectangular, and if the next position (x_{t+1}, y_{t+1}) exits this region, the rollout ends and is counted as a failure. The subsequent discrete state s_{t+1} is computed by re-quantizing $(d_{t+1}, e_{t+1}, v_{t+1}, \omega_{t+1})$ in the same way as before, with d_{t+1} the updated goal distance, e_t and e_{t+1} the heading errors at consecutive steps, v_{t+1} the updated forward speed, and ω_{t+1} the updated angular speed. Therefore the state transition map $\mathcal{P}(\cdot | s, a)$ is deterministic. The objective is to learn a policy $\pi(a | s)$ that maximizes the expected discounted return (2). The per-step reward is defined via a shaped cost that jointly captures goal progress, control smoothness, and stability objectives, as follows:

$$r_t = R(s_t, a_t, s_{t+1}) = R_{\text{task}} + R_{\text{shape}} \quad (7)$$

where s_t and s_{t+1} denote the current and subsequent discrete states, respectively, and a_t is the action applied at time t . The term $R_{\text{task}}(s_t, a_t, s_{t+1})$ represents the primary objective, including

- 1 Step cost: $r_{\text{step}} = -k_{\text{step}}$
- 2 Distance progress: $r_d = k_d(d_t - d_{t+1})$
- 3 Timeout shaping: $r_{\text{timeout}} = -k_{\text{timeout}} d_T$

where $k_{\text{step}} > 0$ discourages unnecessarily long rollouts, $k_d > 0$ scales the incentive for reducing the goal distance, and d_T denotes the remaining distance to the target when a timeout occurs. Collectively, these terms express the core task objective of driving the system toward the goal, as

$$R_{\text{task}} = r_{\text{step}} + r_d + r_{\text{timeout}}, \quad (8)$$

that is, reaching the target promptly while discouraging timeouts that leave the agent far from the goal. The shaping component $R_{\text{shape}}(s_t, a_t, s_{t+1})$ further guides the policy by specifying how the goal should be approached, promoting favorable approach angles, smooth control, and reduced oscillations. The baseline reward is defined as

$$R_{\text{shape}} = r_\theta + r_\omega + r_v^{\parallel} + r_v^{\perp} + r_a + r_{\text{hyst}} + r_{\text{goal}} + r_{\text{flip}} + r_{\text{inc}} + r_{\text{stall}} + r_{\text{stop}} + r_{\text{sign}} \quad (9)$$

Let $a_{v,t}$ and $a_{\omega,t}$ denote the applied linear and angular accelerations. Assume the following positive weighting parameters: k_θ , k_ω , k_v , k_{lat} , k_{a_v} , k_{a_ω} , k_{ws} , k_d , $k_{w\text{flip}}$, $k_{\text{heading,inc}}$, and $k_{\text{heading,stall}}$. The corresponding reward terms are then given by

- 1 $r_\theta = k_\theta(|e_t| - |e_{t+1}|)$
- 2 $r_\omega = -k_\omega \frac{1+\cos(|e_{t+1}|)}{2} \omega_{t+1}^2$
- 3 $r_v^{\parallel} = k_v v_{t+1} (\max(0, \cos(e_{t+1})))^2$
- 4 $r_v^{\perp} = -k_{\text{lat}} v_{t+1}^2 \sin^2(e_{t+1})$
- 5 $r_a = -k_{a_v} a_{v,t}^2 - k_{a_\omega} (0.5 + 0.5 \frac{1+\cos(|e_{t+1}|)}{2}) a_{\omega,t}^2$
- 6 $r_{\text{hyst}} = -k_{ws} \max(0, |\omega_{t+1}| - w_{\text{db}})^2$ if $|e_{t+1}| < e_{\text{db}}$
- 7 $r_{\text{goal}} = k_d d_t$ if $d_{t+1} \leq d_{\text{goalTol}}$
- 8 $r_{\text{flip}} = -k_{w\text{flip}}$ if ω_{t+1} changes sign
- 9 $r_{\text{inc}} = -k_{\text{heading,inc}} \max(0, \Delta e)$
- 10 $r_{\text{stall}} = -k_{\text{heading,stall}} |e_{t+1}|$
- 11 $r_{\text{stop}} = -k_{w\text{stop}} \text{excess}^2$
- 12 $r_{\text{sign}} = -k_{w\text{sign}} \text{wrong}^2$ if $\text{wrong} > 0$

Reward 1 promotes decreasing the heading error, while Reward 2 discourages high angular speeds, with a stronger effect as the robot approaches alignment. Rewards 3 and 4 reduce incentives for forward motion when the heading is poorly aligned. Reward 5 penalizes large accelerations (with a heavier penalty on angular acceleration near alignment), and Reward 6 adds hysteresis to damp residual rotation outside the small deadbands ω_{db} and e_{db} . Reward 7 provides a terminal bonus upon success, and Reward 8 penalizes sign changes in ω near alignment when $|e_{t+1}|$ is small. Let $\Delta e = |e_{t+1}| - |e_t|$; Reward 9 penalizes increases in heading error, and Reward 10 penalizes lack of improvement when $|\Delta e|$ is small but $|e_{t+1}| > 0$. Reward 11 defines the stopping angle $\theta_{\text{stop}} = \omega_{t+1}^2 / (2a_\omega^B)$ and penalizes angular velocities that cannot be reduced to zero within $|e_{t+1}| + e_{\text{pad}}$. Finally, letting $s_0 = \text{sign}(e_0)$, Reward 12 penalizes ω_{t+1} whenever it turns in the opposite direction of s_0 beyond the deadband ω_{db} , thereby encouraging monotonic heading correction. Classical potential-based shaping introduces an auxiliary potential function $\Phi : \mathcal{S} \rightarrow \mathbb{R}$ and defines a shaping term

$$F(s_t, s_{t+1}) = \gamma \Phi(s_{t+1}) - \Phi(s_t), \quad (10)$$

which is combined with a baseline task reward R_{task} to form the overall shaped reward

$$\tilde{R}(s_t, a_t, s_{t+1}) = R_{\text{task}}(s_t, a_t, s_{t+1}) + F(s_t, s_{t+1}). \quad (11)$$

For any $\gamma \in (0, 1)$, this formulation leaves the optimal-policy set of the original MDP unchanged. In our case, the distance-

and heading-progress components can be interpreted through this lens. Define the scalar potential

$$\Phi(s_t) = \Phi(d_t, e_t) = k_d d_t + k_\theta |e_t|. \quad (12)$$

Then the combined distance and heading reward terms satisfy

$$r_d + r_\theta = \Phi(s_t) - \Phi(s_{t+1}). \quad (13)$$

Hence, aside from the sign and the discount factor γ , these terms can be interpreted as the reduction of a potential Φ that assigns higher cost to larger goal distance and larger heading error. In this sense, they play a role analogous to potential-based shaping using a Lyapunov-like function of (d, e) . The other shaping terms (penalties on velocity and acceleration, hysteresis effects, the predictive stopping penalty, the sign-flip penalty, and the wrong-sign penalty) cannot be written in the simple form $\gamma\Phi(s_{t+1}) - \Phi(s_t)$. Rather, they explicitly alter the control criterion by promoting smooth, non-oscillatory, and monotone motion, instead of optimizing only for minimum time-to-goal. The agent uses a tabular action-value function $Q : \mathcal{S} \times \mathcal{A} \rightarrow \mathbb{R}$, initialized at zero. At each step, a temporal-difference (TD) update is performed

$$Q(s_t, a_t) \leftarrow Q(s_t, a_t) + \alpha \delta_t, \quad (14)$$

where $\alpha > 0$ denotes the learning-rate parameter and δ_t is the corresponding TD error. The specific form of δ_t depends on the selected update rule and is given by

- **Q-learning (off-policy):**

$$\delta_t = r_t + \gamma \max_{a' \in \mathcal{A}} Q(s_{t+1}, a') - Q(s_t, a_t), \quad (15)$$

- **SARSA (on-policy):**

$$\delta_t = r_t + \gamma Q(s_{t+1}, a_{t+1}) - Q(s_t, a_t), \quad (16)$$

where $r_t = R(s_t, a_t, s_{t+1})$ is the one-step reward, and a_{t+1} is the subsequent action chosen under the current behavior policy. During learning, actions are sampled using an ε -greedy rule with respect to Q :

$$a_t = \begin{cases} \text{random action} & \text{with probability } \varepsilon_t, \\ \arg \max_{a \in \mathcal{A}} Q(s_t, a) & \text{with probability } 1 - \varepsilon_t, \end{cases} \quad (17)$$

where the exploration parameter ε_t is exponentially annealed from ε_0 to $\varepsilon_{\text{final}}$ across training episodes, whereas evaluation is performed with a fully greedy policy (i.e., $\varepsilon_t = 0$). Beyond reward shaping, two additional policy-level rules explicitly regulate the angular motion near the desired heading and the goal. If the agent is nearly aligned and rotating slowly ($|e_t| < e_{\text{db}}$ and $|\omega_t| < \omega_{\text{db}}$), the angular acceleration is forced to $a_{\omega,t} = 0$ to remove small oscillations. Moreover, inside a small neighborhood of the goal ($|e_t| \leq e_{\text{lock}}$ and $d_t \leq d_{\text{lock}}$), extra constraints are imposed: during training, a bounded braking action is applied to bring ω_t toward zero within acceleration limits, while during evaluation a hard clamp sets $\omega_{t+1} = 0$ and the linear motion still follows the chosen $a_{v,t}$. Equivalently, this yields an

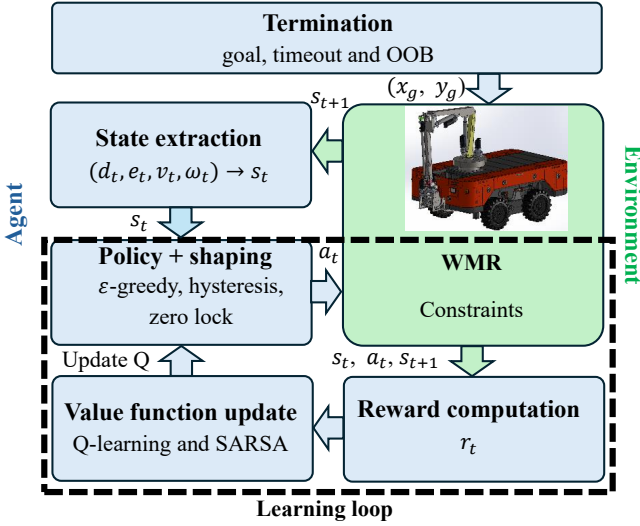


Fig. 1. Architecture of the benchmark RL policy π^0 .

MDP with state-dependent action constraints and altered transition behavior close to the goal, introduced to stabilize the learned policy and remove residual heading oscillations.

Fig. 1 summarizes the closed-loop RL architecture for WMRs. At each step, the agent extracts the state s_t from measured signals, selects an action a_t using an ϵ -greedy policy with shaping (hysteresis and zero-lock), and applies it to the constrained robot dynamics to obtain the next state s_{t+1} . The reward r_t is computed from the transition, the Q function is updated using Q-learning or SARSA, and the episode terminates when the goal is reached or when a timeout or out-of-bounds (OOB) condition occurs.

4. Lyapunov-Like Stabilizer Agent Design

Given the benchmark RL goal-reaching policy π^0 designed in Section 3, here, we aim to design a stabilizer agent to improve its performance efficiently while provably maintaining the same goal-reaching guarantee.

Definition 4.1. [19]: The benchmark goal-reaching policy $\pi^0 \in \Pi$ constructed in Section 3 satisfies the allowed failure probability $\eta \in [0, 1)$, if we have

$$\mathcal{P}\left(\lim_{t \rightarrow \infty} d_t(P_t, X_G) \xrightarrow{t \rightarrow \infty} 0 \mid A_t \sim \pi^0(S_t)\right) \geq 1 - \eta \quad (18)$$

for every initial condition $s_0 \in \mathcal{S}$ where $d_t(P_t, X_G)$ is the distance of robot pose P_t to the goal pose X_G at t . That is, the policy π^0 fails to reach the goal at most η .

Now we seek to improve the designed goal-reaching RL policy π^0 using collected data. We enforce Lyapunov-like constraints only during critic updates, and we use a fallback mechanism when the constrained update is infeasible. Concretely, at time t , we first compute a greedy action under the last accepted critic, $a^* \in \arg \min_{a \in \mathcal{A}} \hat{Q}^{w^*}(s_t, a)$, and then attempt a constrained critic update, including the decrease constraint, defined as

$$w^* \in \arg \min_{w \in \mathcal{W}} L_{\text{crit}}(w) \quad \text{s.t.} \quad \hat{Q}^w(s_t, a_t) - \hat{Q}^{w^*}(s^*, a^*) \leq -\bar{v} \quad (19)$$

Here, $\hat{Q}^w(s, a)$ is the critic (an action-value, discounted cost-to-go approximation) parameterized by $w \in \mathcal{W}$, w^* denotes the last accepted critic parameters, and w^* is the candidate updated critic parameters returned by the constrained optimization. The tuple (s^*, a^*) is the stored reference state-action pair, initialized as (s_0, a_0) with $w^* \leftarrow w_0$, and updated after each successful critic update as $(s^*, a^*, w^*) \leftarrow (s_t, a^*, w^*)$.

Define an embedding $\phi: \mathcal{S} \rightarrow \mathcal{R}^n$. For the \mathcal{K}_∞ bounding functions, a practical selection is to use quadratic forms as

$$\hat{\kappa}_{\min}(\|\phi(s_t)\|) \leq \hat{Q}^w(s_t, a_t) \leq \hat{\kappa}_{\max}(\|\phi(s_t)\|) \quad (20)$$

where for a nonnegative scalar ϵ

$$\hat{\kappa}_{\min}(\epsilon) = C_{\min} \epsilon^2, \quad \hat{\kappa}_{\max}(\epsilon) = C_{\max} \epsilon^2 \quad (21)$$

note that $0 < C_{\min} < C_{\max}$. If the constraints in Eqs. 19 and 20 hold, the resulting Lyapunov-style condition guarantees that the system reaches X_G , in the same spirit that a Lyapunov function provides a certificate of goal reaching. If the constrained problem has no feasible solution, the Lyapunov-like critic function falls back to the benchmark policy π^* by sampling $a_t \sim \pi_{0,t}(\cdot | s_t)$, and it suspends learning-driven action selection until the system returns to a smaller neighborhood of the goal where the critic update becomes feasible again. Finally, $\bar{v} > 0$ is a hyperparameter that enforces a minimum decrease in the critic value between successive successful updates. Note that the constraints are always feasible in a sufficiently small neighborhood of the goal, provided the critic is sufficiently expressive and $\hat{Q}^{w^*}(s^*, a^*) > \bar{v}$.

Taken together, the parameters $\hat{\kappa}_{\min}$, $\hat{\kappa}_{\max}$, and \bar{v} set the balance between how permissive learning and exploration can be and how large the worst-case time-to-goal may become. In particular, both the ratio $\frac{C_{\min}}{C_{\max}}$ and the threshold \bar{v} influence the exploration-versus-conservatism trade-off and therefore the worst-case reaching time. The critic training loss $\mathcal{L}^{\text{crit}}$ as a function of critic weights w is also user-defined. One option is an on-policy 1-step Temporal Difference (TD) loss:

$$\mathcal{L}^{\text{crit}}(w) = \sum_{k=0}^{T_\xi} \left(\hat{Q}^w(s_{t_k}, a_{t_k}) - C(s_{t_k}, a_{t_k}) - \hat{Q}^{w^*}(s_{t_{k+1}}, a_{t_{k+1}}) \right)^2 + \chi_{\text{crit}}^{-2} \|w - w^*\|^2 \quad (22)$$

where $k = 0, \dots, T_\xi$ is index over a rollout (trajectory segment) ξ of length T_ξ . t_k is the time-step index in the rollout at position k (so (s_{t_k}, a_{t_k}) is the k -th state-action pair). χ_{crit} is the critic step-size / regularization scale. Note that if the optimization is done with gradient descent, the weight-change penalty $\chi_{\text{crit}}^{-2} \|w - w^*\|^2$ is often unnecessary, because a learning rate χ_{crit} can control step size directly. Importantly, the specific critic loss (or the choice of learning rate) does not alter the theoretical guarantee of reaching X_G , although it can affect learning efficiency and solution quality. While the expression above resembles SARSA because it uses on-policy next actions, the agent does not require an on-policy update. Off-policy variants are also valid, for example by replacing $a_{t_{k+1}}$ with a greedy action.

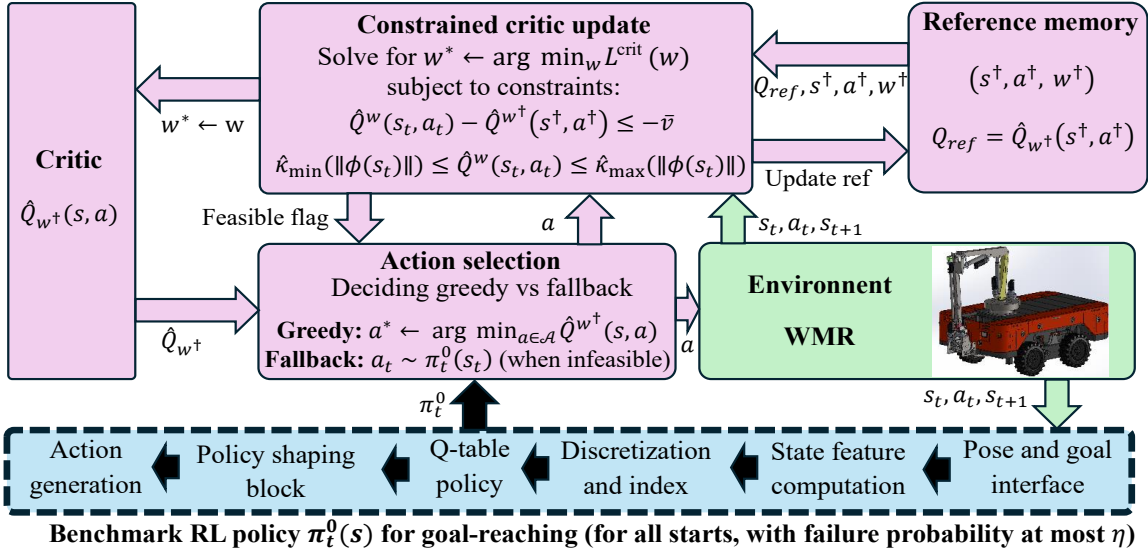


Fig. 2. Lyapunov-Like Stabilizer Agent Framework as the additional layer of the benchmark RL designed in Section 3.

The agent's ability to reuse prior knowledge can be understood in a few ways. To start, any policy that fails to reach the goal is ruled out, which greatly reduces the set of behaviors the learner needs to explore. There is also a subtler mechanism at work: whenever the nominal policy π^0 is executed for a run of N state action steps, the critic is adjusted so that the initial state action pair of that run is assigned the cumulative cost incurred under the nominal policy plus the estimated value at the end of the run:

$$\hat{Q}(s^, a^) \leftarrow \sum_{i=0}^{N-1} C(s_i, a_i) + \hat{Q}(s_N, a_N), \quad a_i \sim \pi_{t^+i}^0 \quad (23)$$

where in $a_i \sim \pi_{t^+i}^0$: each a_i is sampled from the nominal (benchmark) policy π^0 at time $t^+ + i$. t^+ is the time index when that nominal-policy segment starts. The procedure establishes an initial safety margin that later episodes can shrink, in the same spirit as repeated backup operations that continually improve earlier value bounds. As a result, the learned agent not only maintains the guarantee of reaching the goal, but also inherits useful information from the benchmark RL policy π^0 during training.

Remark 4.1. In contrast to BF-based approaches that irrevocably exclude some state-action combinations, the proposed stabilizer does not make any combination inherently unreachable. Even if a poor choice causes π^0 to hand over control immediately afterward, the consequences of that choice remain observable and therefore can still be learned from.

Remark 4.2. The level of conservatism is adjustable through \bar{v} . Smaller \bar{v} means weaker constraints, less restrictive learning, and more permissive exploration. In fact, with sufficiently small \bar{v} and a reasonable critic architecture (for instance, one with an output-layer bias or the ability to locally approximate constant functions), any finite sequence of state-action decisions can be executed without forcing an interruption.

Remark 4.3. The goal-reaching does not depend on delicate hyperparameter tuning. It is maintained for any hyperparameter

values, provided the benchmark RL policy π^0 already reaches the goal and $\bar{v} > 0$.

Remark 4.4. The stabilizer agent is intentionally modular and can accommodate any critic objective, action update rule, exploration strategy, or optimizer, as long as constraint satisfaction is verified and violations are detected. These choices do not change the agent's formal goal-reaching guarantee.

Figure 2 illustrates a Lyapunov-like safe RL loop at each state s_t , the agent proposes a greedy action a^* from the learned critic \hat{Q}_{w^*} , then attempts a constrained critic update that enforces a Lyapunov-like decrease relative to a stored reference value Q_{ref} and state-dependent value bounds $\hat{k}_{min} \leq \hat{Q}^w(s_t, a^*) \leq \hat{k}_{max}$. If the constraints are feasible, the greedy action is executed, and the reference memory is updated; otherwise, the agent falls back to the benchmark goal-reaching policy π^0 , which (as in Section 2.2) is designed using Q-learning and SARSA while explicitly respecting practical robot limits to generate continuous, well-behaved commands. In this way, the trained RL model is integrated with the Lyapunov-like stabilizer to preserve safe behavior during learning and provide formal convergence guarantees.

5. Formal Guarantee Analysis

Define $S_t^\pi(s_0)$ as the (random) state sequence that starts at s_0 and evolves under policy $\pi \in \Pi$. In particular, $S_0^\pi(s_0) = s_0$. For $t > 0$, the next state is drawn from the transition model,

$$S_t^\pi(s_0) \sim \mathcal{P}(\cdot | S_{t-1}^\pi(s_0), A_{t-1}(s_0)) \quad (24)$$

where the action is sampled from the policy,

$$A_{t-1}(s_0) \sim \pi_{t-1}(\cdot | S_{t-1}^\pi(s_0)) \quad (25)$$

The key guarantee about keeping the goal-reaching behavior is stated next.

Theorem 5.1. Consider Eqs. 1 and 2 and $\eta \in [0, 1)$. Assume $\pi^0 \in \Pi$ reaches the goal set $X_G \subset \mathcal{S}$ in the sense that for all $s_0 \in \mathcal{S}$

$$\mathcal{P}\left(\lim_{t \rightarrow \infty} d_t(P_t^{\pi^0}(s_0), X_G) \xrightarrow{t \rightarrow \infty} 0\right) \geq 1 - \eta \quad (26)$$

If π_t be the policy generated by the proposed stabilizer agent, for all $t \geq 0$, the same type of goal-reaching guarantee holds for π_t , namely

$$\mathcal{P}\left(\lim_{t \rightarrow \infty} d_t(P_t^{\pi^t}(s_0), X_G) \xrightarrow{t \rightarrow \infty} 0\right) \geq 1 - \eta \quad (27)$$

Proof. Following the proposed agent, write

$$\hat{Q}^\dagger := \hat{Q}^{w^\dagger}(s^\dagger) \quad (28)$$

Define the set of time indices where the critic update succeeds:

$$\hat{\mathcal{T}}(w) := \{t \in \mathcal{Z}_{\geq 0}\} \quad (29)$$

These are exactly the times when the critic accepts an update and the resulting action is applied at the next step. The complementary times are those where the critic fails first, with any immediately following failures ignored. Now define a "held" critic value:

$$\hat{Q}_t^\dagger := \begin{cases} \hat{Q}_t, & t \in \hat{\mathcal{T}} \\ \hat{Q}_{t-1}^\dagger, & \text{otherwise.} \end{cases} \quad (30)$$

we will have

$$\hat{T} := \max \left\{ \frac{\hat{Q}_0^\dagger - \bar{v}}{\bar{v}}, 0 \right\} \quad (31)$$

where \hat{T} is a (deterministic) upper bound on how many successful critic updates can happen before updates must stop and the algorithm falls back to the baseline π^0 forever. Therefore $\hat{\mathcal{T}}(w)$ is finite. Also, \hat{T} does not depend on X_G ; it depends only on the critic's initial value. Let $t_{\text{final}}^\dagger(w) = \sup \hat{\mathcal{T}}(w)$ be the last time a successful critic update occurs. For any $\tau \geq 0$, once $t_{\text{final}}^\dagger = \tau$, all later actions satisfy $A_{\tau+t+1} \sim \pi^0(S_{\tau+t}^{\pi^t}(s_0))$. By the theorem's assumption on π^0 , this implies

$$\mathcal{P}\left(\lim_{t \rightarrow \infty} d_t\left(P_{t_{\text{final}}^\dagger + t}^{\pi^t}, X_G\right) \xrightarrow{t \rightarrow \infty} 0 \mid t_{\text{final}}^\dagger = \tau\right) \geq 1 - \eta \quad (32)$$

We can apply the total probability law, as

$$\begin{aligned} & \mathcal{P}\left(\lim_{t \rightarrow \infty} d_t\left(P_{t_{\text{final}}^\dagger + t}^{\pi^t}, X_G\right) \xrightarrow{t \rightarrow \infty} 0\right) \\ &= \sum_{\tau=0}^{\infty} \mathcal{P}[\cdots \mid t_{\text{final}}^\dagger = \tau] \mathcal{P}[t_{\text{final}}^\dagger = \tau] \\ &\geq (1 - \eta) \sum_{\tau=0}^{\infty} \mathcal{P}[t_{\text{final}}^\dagger = \tau] = 1 - \eta \end{aligned} \quad (33)$$

This completes the proof. In short, the theorem shows that the agent continues to reach the goal even while learning online.

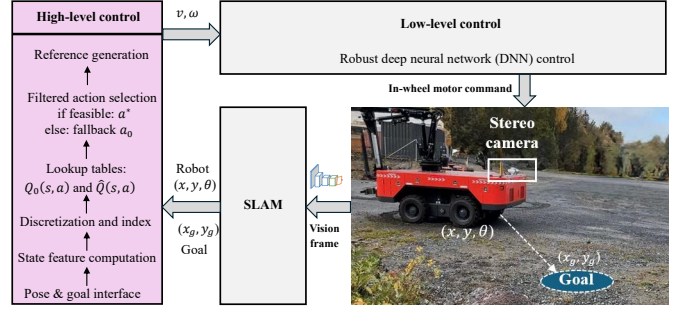


Fig. 3. The proposed RL policy enhanced by the stabilizer agent within the whole experimental framework.

Table 1 Parameters of the benchmark RL π^0 .

Parameter	Value	Description
dt	0.05	time step (s)
episodes	30000	Training ep
evalEpisodes	1000	Greedy eval ep
goalTol	0.10	tol radius (m)
startMinDistToGoal	0.20	Min. start dis. to goal (m)
$[x, y]$ bounds	$[-25, 25]$	Space bounds (m)
$[\Delta x, \Delta y]$	$[1.0, 1.0]$	Grid resolution (m)
n_θ	24	Heading bins
$[N_v, N_\omega]$	$[4, 5]$	Velocity bins
$[v_{\min}, v_{\max}]$	$[0.0, 0.25]$	Lin. speed (m/s)
$[\omega_{\min}, \omega_{\max}]$	$[-0.15, 0.15]$	Ang. speed (rad/s)
$[a_{v,\min}, a_{v,\max}]$	$[-0.10, 0.10]$	Lin. acc. (m/s ²)
$[a_{\omega,\min}, a_{\omega,\max}]$	$[-0.02, 0.02]$	Ang. acc. (rad/s ²)
$[\Delta a_v, \Delta a_\omega]$	$[0.10, 0.02]$	Acc. grid [m/s ² , rad/s ²]
e_{db}	0.01	Hys. heading (rad)
ω_{db}	0.001	Hys. ang. (rad/s)
k_{ws}	1.2	Hys. spin penalty gain
e_{lock}	0.03	Zero lock heading (rad)
d_{lock}	0.30	Zero lock distance (m)
α	0.10	Learning rate
γ	0.95	Discount factor
$[\varepsilon_0, \varepsilon_{\text{final}}]$	$[1.0, 10^{-3}]$	Exploration rate

6. Validating Results

This section evaluates the efficacy of the proposed RL approach, augmented with a stabilizer agent, on a real-world platform: a 6000 kg skid-steering off-road WMR. This robot is equipped with stereo RGB cameras (global shutter, 0.32 m baseline, pitched 5° downward), a high-precision Trimble BD992 INS/RTK unit, and wheel-speed sensors, with all data recorded on a Beckhoff PC. The cameras are meticulously calibrated using Kalibr and captured in uncompressed format for stereo ORB-SLAM3, configured for roughly 2,000 features per frame, a 40 m stereo depth cutoff, and a FAST detector threshold of 12 px. The complete robot framework is illustrated in Fig. 3, which summarizes the practical navigation and control architecture and highlights the proposed high-level control module (shown in pink).

In this work, the high-level controller executes a trained RL policy, π^0 , represented by a tabular $Q_0(s, a)$ over a discretized state $s = [d_t, e_t, v, \omega]$. It is further complemented by a stabilizer cost-critic, $\hat{Q}(s, a)$, which refines decision making through filtered action selection. When the agent's feasibility condition is satisfied, the controller selects the stabilizing action $a^* = \arg \min_a \hat{Q}(s, a)$; otherwise, it safely falls back to the baseline action $a_0 = \arg \max_a Q_0(s, a)$. This module also includes the pose and goal interface, state-feature computa-

Table 2 Stabilizer refinement and online rollout parameters.

Group	Parameter	Value
Stabilizer refine	episodes	2000
Stabilizer refine	α_{crit}	0.1
Stabilizer refine	γ	0.95
Stabilizer refine	$\tilde{\gamma}$	1×10^{-2}
K ∞ bounds	C_{low}	0.1
K ∞ bounds	C_{up}	500
Simulation	Δt_{policy}	0.05
Simulation	Δt_{sim}	0.001
Normalization	d_{scale}	35.36
Cost weights	w_d	1.0
Cost weights	w_e	0.1
Cost weights	w_u	0.01

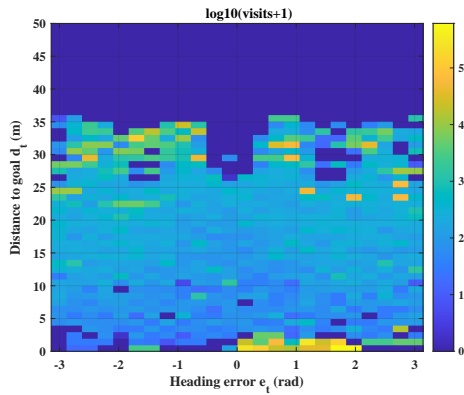


Fig. 4. Visitation and cost-to-go over the (d_t, e_t) grid for the most frequently visited (v, ω) slice ($v \approx 0.025$, $\omega \approx 0$).

tion, discretization and indexing, and reference generation, ultimately outputting velocity references (v, ω) to the rest of the system. The remaining components follow established implementations. Robot pose (x, y, θ) and goal information (x_g, y_g) are provided by a SLAM subsystem based on ORB-SLAM3 [21]. Low-level control tracks the (v, ω) references using a supervised deep neural network in-wheel actuator model, robustified via adaptive control, as in [22]. The benchmark goal-reaching RL policy π^0 was trained in MATLAB, using the parameter settings and constraints specified in Table 1.

The parameter settings related to the stabilizer refinement used in MATLAB are shown in Table 2.

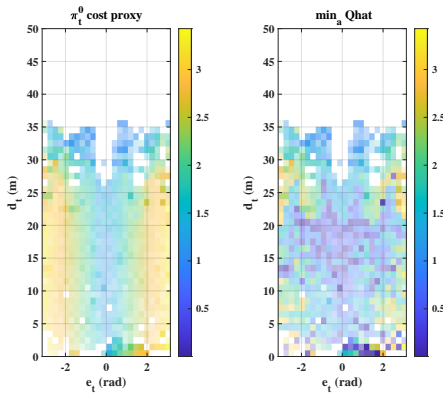


Fig. 5. Comparison between the benchmark RL cost proxy (left) and stabilizer critic $\min_a \hat{Q}(s, a)$ (right).

Table 3 Comparison between the benchmark RL and the stabilizer.

Metric	Benchmark RL	Stabilizer
Success rate (%)	84.6	99.0
Goal end (%)	84.6	99.0
Timeout end (%)	15.2	1.0
Out of bounds end (%)	0.2	0.0
Steps (all eps), median	1875	1554
Steps (all eps), mean	2314.1	1561.8
Steps, median (success)	1737	1548
Steps, mean (success)	1790.1	1524.9
Final dis, median (all)	0.096	0.095
Final dis, mean (all)	4.669	0.375
Final dis, median (fail)	31.566	31.566
Final dis, mean (fail)	29.798	28.063
Fallbacks, median	—	1457
Fallbacks, mean	—	1456.4
Fallbacks/steps, mean	—	0.920

6.1. Numerical Results

This section evaluates the proposed RL policies in simulation. The visitation heatmap in Fig. 4 indicates which (d_t, e_t) regions are actually encountered during rollouts for the selected (v, ω) slice, and therefore where the learned values are supported by experience. The heatmaps are shown for the (v, ω) discretization slice with the highest empirical visitation count, and in this experiment the most frequently visited bin corresponds to the bin-center values $v \approx 0.025$ m/s and $\omega \approx 0$ rad/s. The $\log_{10}(\text{visits}+1)$ transform is applied only to the visitation heatmap to compress the wide dynamic range of visit counts and make both highly visited and sparsely visited bins visible within a single color scale. In the visitation study, one goal is sampled uniformly at random per rollout episode, so the total number of randomly chosen goals equals the number of episodes (e.g., 2000 goals for 2000 episodes). The concentration of visits below approximately 35 m arises because the start state is at the origin and goals are sampled within the square workspace bounds, so the maximum possible initial distance is approximately the distance from the origin to a corner, $\sqrt{25^2 + 25^2} \approx 35.36$ m (for bounds $[-25, 25]$). As shown in Fig. 5, within these frequently visited bins (high $\log_{10}(\text{visits}+1)$), the Lyapunov-like stabilizer critic $\min_{a \in \mathcal{A}} \hat{Q}(s, a)$ is typically lower than the benchmark-derived cost proxy, indicating that the Lyapunov-like stabilizer reshapes the value landscape toward a smaller predicted cumulative penalty in terms of distance-to-goal d_t , heading error e_t , and control effort. Importantly, the Lyapunov-like stabilizer’s refinement is performed only when the monotone improvement constraint is feasible; when it is not, the algorithm reverts to the benchmark policy, thereby preventing unsafe or unsupported updates. As a result, the most reliable differences between the benchmark and Lyapunov-like stabilizer heatmaps occur in the well-visited region, providing visual evidence of the Lyapunov-like stabilizer’s central principle: improve the policy where the constraint can be satisfied, and otherwise fall back to the benchmark to preserve goal-reaching behavior.

Table 3 reports comparative performance over $N = 2000$ matched-goal rollouts, where the same randomly sampled goals

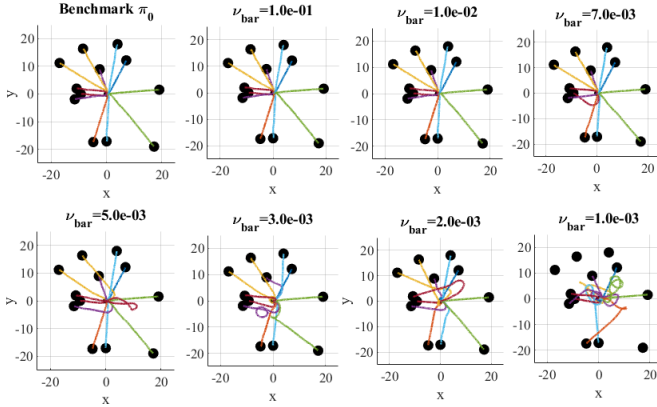


Fig. 6. Overlaid trajectories from the origin to 12 random goal locations.

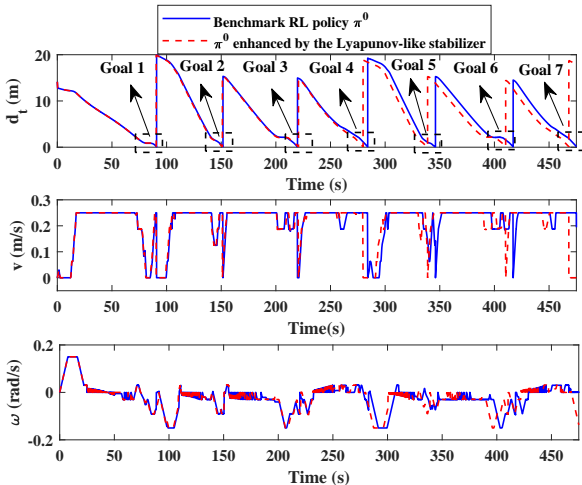


Fig. 7. Overlaid trajectories from the origin to 12 random goal locations.

are evaluated under the benchmark RL policy π_0 (greedy $\arg \max Q_0$) and the Lyapunov-like stabilizer, which applies the refined action only when the monotone improvement constraint is feasible and otherwise falls back to π_0 . Relative to π_0 , the stabilizer increases the goal-reaching rate from 84.6% to 99.0% primarily by reducing timeouts from 15.2% to 1.0%, while also eliminating out-of-bounds terminations (from 0.2% to 0.0%). In addition, the stabilizer improves efficiency, reducing the overall median and mean episode lengths (1875 to 1554 steps, and 2314.1 to 1561.8 steps) and also reducing steps-to-goal among successful episodes (median 1737 to 1548, mean 1790.1 to 1524.9). The final-distance statistics further reflect the reduction in failures: the median final distance remains near the goal tolerance for both methods (about 0.095 m), but the mean final distance over all episodes drops substantially under the stabilizer (4.669 m to 0.375 m) because far-from-goal timeouts become rare. Finally, the fallback statistics indicate that the stabilizer is conservative in deployment, reverting to π_0 for most control steps (mean fallbacks/steps ≈ 0.920), yet the remaining interventions are sufficient to markedly improve goal-reaching without sacrificing safety.

Figure 6 compares benchmark π_0 and the stabilizer for multiple $\bar{\nu}$ settings on the same set of 12 randomly sampled goal

locations, with all rollouts starting from the origin. Each panel overlays the resulting trajectories to these goals, so differences in path shape reflect only the policy, not different goal samples. Overall, the stabilizer preserves the benchmark’s goal-reaching behavior while altering the motion patterns in a $\bar{\nu}$ -dependent way: larger $\bar{\nu}$ typically yields trajectories that remain closer to π_0 , while smaller $\bar{\nu}$ allows more deviation from the benchmark, which can appear as tighter turns or more noticeable path reshaping before converging toward the goal. This visualization therefore provides a direct qualitative check that agent’s stabilizing updates modify trajectories systematically while maintaining consistent performance across identical goal instances.

The simulation results of the robot tasks are illustrated in Fig. 8. In this experiment, we consider seven randomly moving (nonstationary) goals whose speeds are lower than the robot’s maximum speed. Although the goals evolve stochastically, the proposed rRL policy augmented with a Lyapunov-like stabilizer progressively reduces the robot–goal distance over time and ultimately reaches each goal.

Figure 7 presents the key comparative signals for the first three goals using the nominal policy π_0 and the enhanced policy, evaluated under the same set of randomly moving goals from the simulation in Fig. 8. The plotted signals include the robot–goal distance, as well as the robot’s linear and angular velocities. For the first three goals, both controllers exhibit similar behavior initially; however, after some time, the nominal policy becomes slower in reaching the goals. This difference is consistent with the velocity profiles: augmenting the RL policy π_0 with the Lyapunov-like stabilizer enables the robot to sustain higher velocities for longer while reducing oscillations, which improves goal-reaching performance.

6.2. Experimental Results

The proposed RL approach, augmented with a stabilizer agent, was implemented and validated on a real-world platform: a 6000 kg skid-steering WMR. The complete robot framework was illustrated in Fig. 3, which summarizes the practical navigation and control architecture and highlights the proposed high-level control module (shown in pink). As shown in Fig. 9, for the experiments, three stationary goal locations were defined at Goal 1, $(x_g, y_g) = (3, 6)$, Goal 2, $(x_g, y_g) = (3, -6)$, and Goal 3, $(x_g, y_g) = (3, -18)$ on soft, slip-prone terrain, which introduced severe disturbances to the system.

Figures 10, 11, and 12 present the robot pose trajectories recorded by the SLAM module. In each figure, the trajectory shown on a white background corresponds to the zoomed-out (far-view) $x - y$ path, while the trajectory shown on a gray background provides a zoomed-in view. Both policies, π_0 and the enhanced π_0 , successfully reach the specified goals while satisfying the imposed constraints. However, the enhanced policy additionally provides formal goal-reaching guarantees. Moreover, the results indicate that, particularly for Goal 3 (the longest-distance task), the oscillations of the proposed RL policy augmented with the Lyapunov-like stabilizer are substantially smoother and reduced compared with the benchmark π_0 policy.

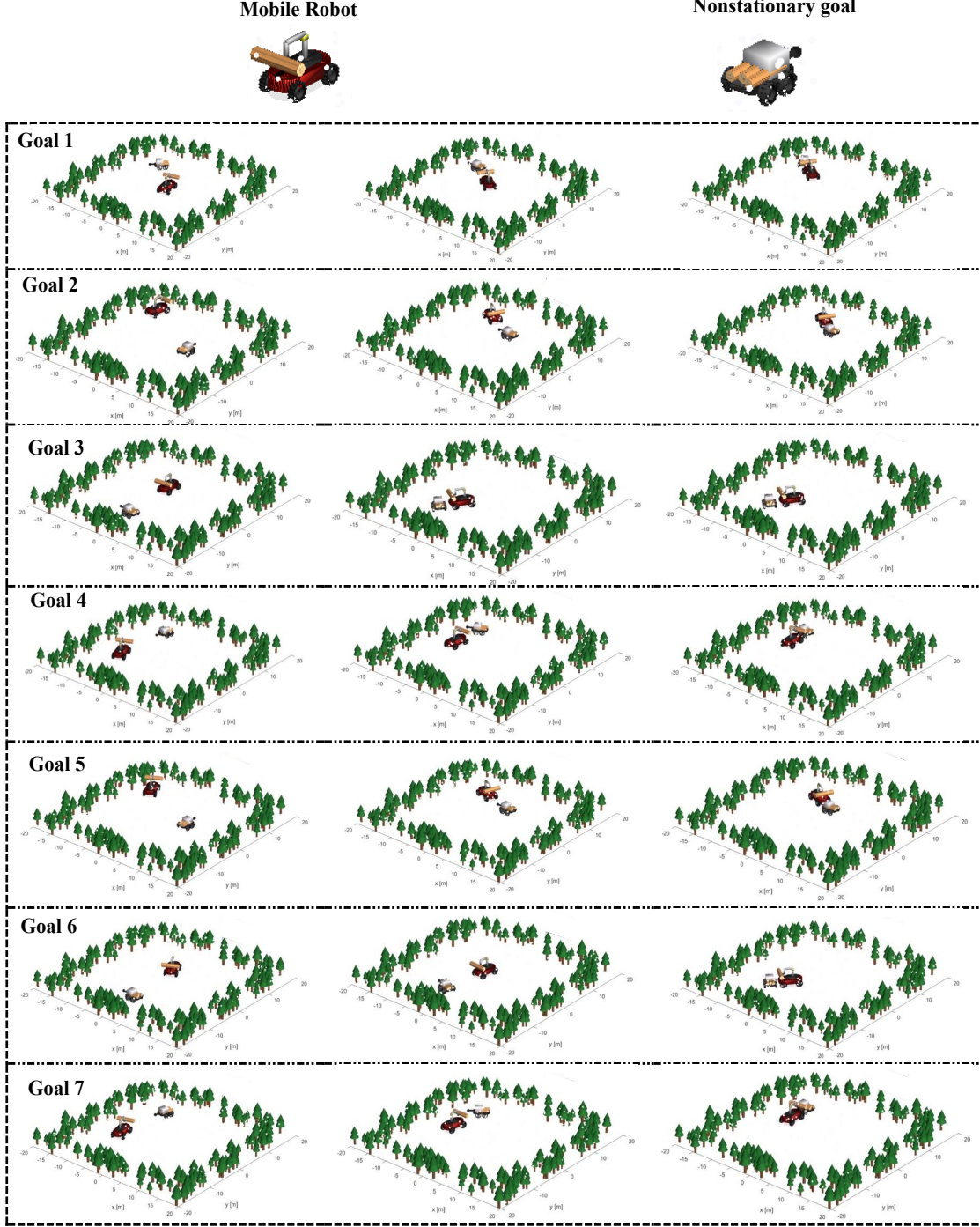


Fig. 8. Closed-loop simulation with seven stochastic, time-varying goal positions. The controller combines the proposed RL goal-reaching policy π^0 with the Lyapunov-like stabilizer agent for enhanced control under nonstationary objectives.

The robot velocity profiles for the three tasks are presented in Figures 13, 14, and 15. An examination of these results indicates that both the linear and angular velocities exhibit smooth trajectories, which is particularly important for visual SLAM performance, as it depends on motion smoothness. In addition, because Goal 3 involves a substantially longer travel distance than the other goals, the robot requires more time to reach the target, since the motion trajectories are constrained by the reinforcement learning policies.

Table 4 compares Pure Pursuit, the benchmark RL policy, and the Lyapunov-like stabilizer enhanced RL policy for the same application and goals. It shows that all three achieve high motion smoothness, with final distance errors of 8.0 cm (Pure Pursuit) and about 5 cm for both RL methods. In terms of efficiency, Pure Pursuit has the longest mean reaching time and highest control effort (69.01 s, 5.10), while the benchmark RL improves both (61.33 s, 4.25), and the enhanced RL further reduces them to 58.33 s and 4.01, respectively. Note that for con-

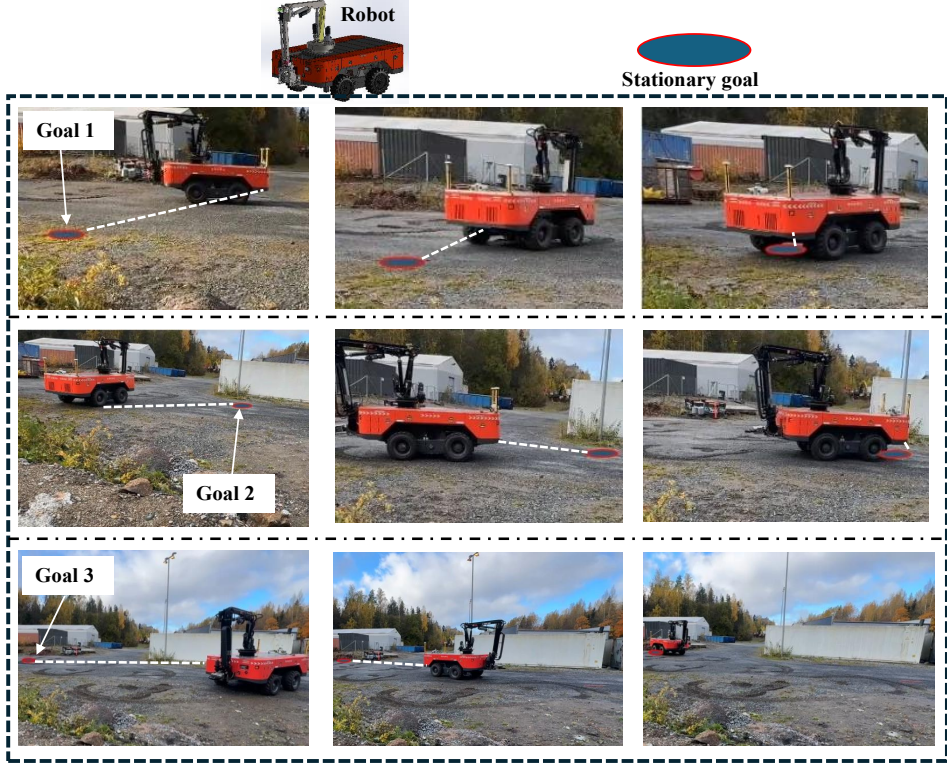


Fig. 9. Closed-loop experiment with three stationary goal positions. The high-level control combines the proposed RL goal-reaching policy π^0 with the Lyapunov-like stabilizer agent for enhanced control under stationary objectives.

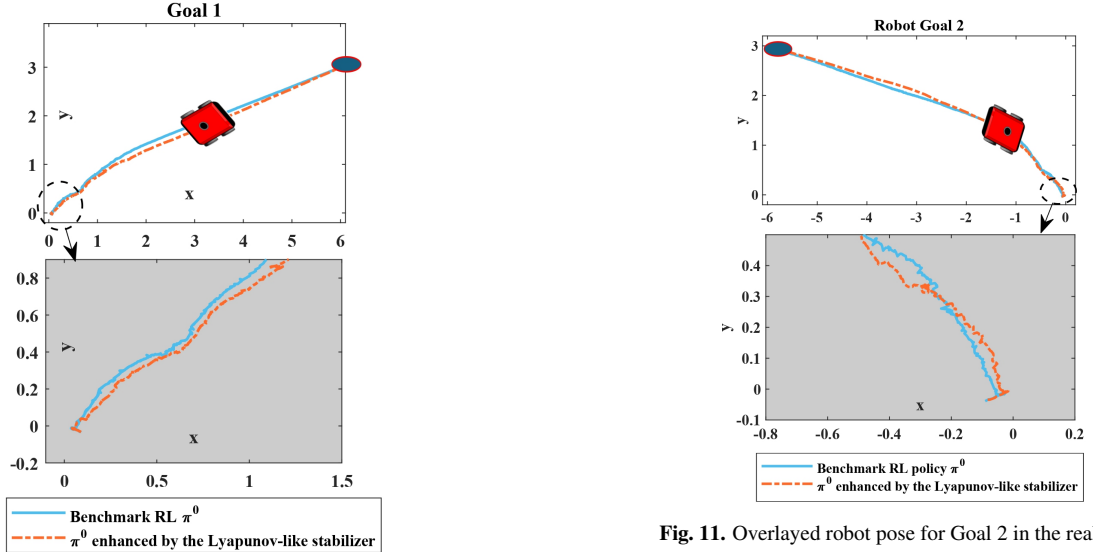


Fig. 10. Overlayed robot pose for Goal 1 in the real world.

control effort metrics, we used the command-energy proxy

$$\bar{E} = \int_0^T (v(t)^2 + \lambda \omega(t)^2) dt, \quad \lambda = \left(\frac{v_{\max}}{\omega_{\max}} \right)^2 \quad (34)$$

with $v_{\max} \approx 0.25$ m/s and $\omega_{\max} \approx 0.15$ rad/s (so $\lambda \approx 2.78$).

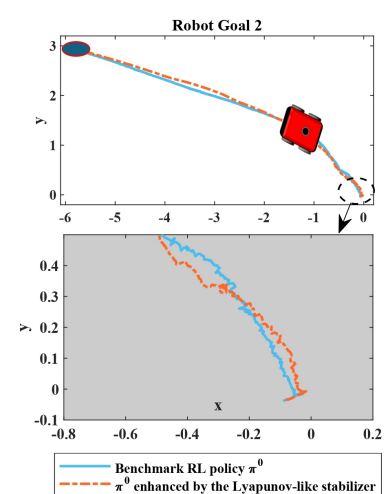


Fig. 11. Overlayed robot pose for Goal 2 in the real world.

7. Conclusion

This paper presented a formal-guaranteed goal-reaching RL framework for real-time on large WMRs operating in slippery, unstructured environments. A smooth, vision-driven RL policy was developed using acceleration-based actions and explicit motion constraints with a set of 12 rewards to generate well-behaved commands under uncertainty. A Lyapunov-like stabilizer layer was then integrated to provide formal convergence guarantees to the goal set without requiring prior knowl-

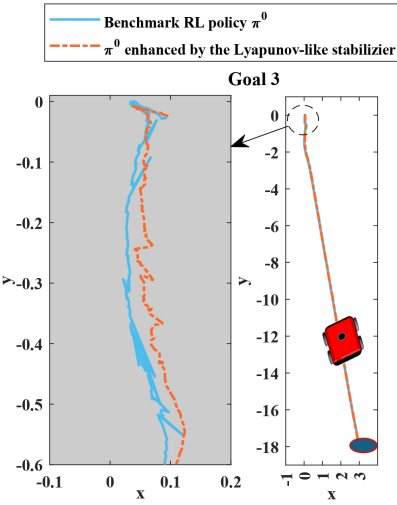


Fig. 12. Overlayed robot pose for Goal 3 in the real world.

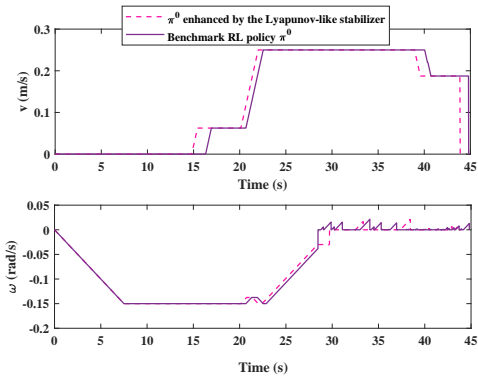


Fig. 13. Overlayed velocity trajectories for Goal 1 in the real world.

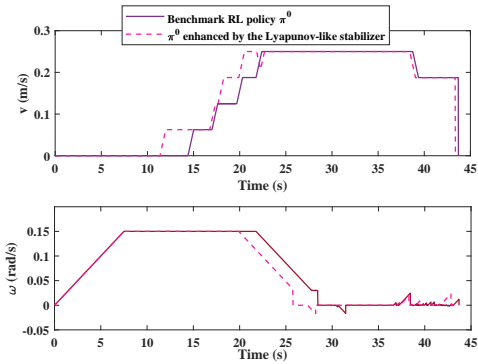


Fig. 14. Overlayed velocity trajectories for Goal 2 in the real world.

edge of a Lyapunov function, while avoiding overly conservative shielding that restricts exploration. Experimental results on a 6,000 kg skid-steer robot demonstrate reliable goal reaching with improved stability and smoother behavior in challenging off-road conditions. Across matched-goal rollouts, the Lyapunov-like stabilizer consistently outperformed the benchmark RL policy, raising the goal-reaching rate from 84.6% to 99.0%, markedly reducing failures, and improving efficiency by

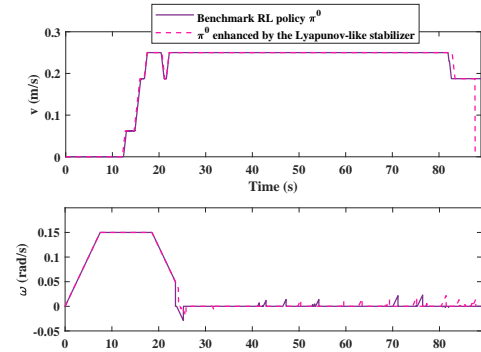


Fig. 15. Overlayed velocity trajectories for Goal 3 in the real world.

Table 4 Comparison of goal-reaching results in the same applications (mean)

Goal-reaching Strategy	Final distance Error (cm)	Motion Smoothness	Reaching time (s)	Control effort (cost)
Pure Pursuit [23]	8.0	high	69.01	5.10
Benchmark RL	5.5	high	61.33	4.25
Enhanced RL	4.7	high	58.33	4.01

shortening both episode length and steps-to-goal while maintaining safe, conservative fallback behavior. Comparative results also showed high performance in the proposed strategy in terms of accuracy and control effort.

CRediT authorship contribution statement

Mehdi Heydari Shahna: Writing - original draft, Validation, Methodology, Investigation, Formal analysis, Software, Data curation, Conceptualization.

Seyed Adel Alizadeh Kolagar: Writing - review & editing.

Jouni Mattila: Writing - review & editing, Resources, Supervision, Funding acquisition.

Declaration of competing interest

The authors declare that they have no known competing financial interests or personal relationships that could have appeared to influence the work reported in this paper.

Acknowledgement

This work was supported by the Business Finland Partnership Project, ‘Future All-Electric Rough Terrain Autonomous Mobile Manipulators’ under Grant No. 2334/31/2022.

References

- [1] P. Henderson, R. Islam, P. Bachman, J. Pineau, D. Precup, D. Meger, Deep reinforcement learning that matters, in: Proceedings of the AAAI conference on artificial intelligence, Vol. 32, 2018.

[2] D. S. Kushwaha, Z. A. Biron, A review on safe reinforcement learning using lyapunov and barrier functions, arXiv preprint arXiv:2508.09128 (2025).

[3] S. Gu, L. Yang, Y. Du, G. Chen, F. Walter, J. Wang, A. Knoll, A review of safe reinforcement learning: Methods, theories and applications, *IEEE Transactions on Pattern Analysis and Machine Intelligence* (2024).

[4] Artificial intelligence — functional safety and ai systems, Tech. Rep. ISO/IEC TR 5469:2024, International Organization for Standardization (2024). URL <https://www.iso.org/standard/81283.html>

[5] M. H. Shahna, P. Mustalahti, J. Mattila, Anti-slip ai-driven model-free control with global exponential stability in skid-steering robots, in: 2025 IEEE/RSJ International Conference on Intelligent Robots and Systems (IROS), 2025, pp. 6855–6862. doi:10.1109/IROS60139.2025.11247584.

[6] Z. Ma, C. Wang, Y. Niu, X. Wang, L. Shen, A saliency-based reinforcement learning approach for a uav to avoid flying obstacles, *Robotics and Autonomous Systems* 100 (2018) 108–118.

[7] Y. Emam, G. Notomista, P. Glotfelter, Z. Kira, M. Egerstedt, Safe reinforcement learning using robust control barrier functions, *IEEE Robotics and Automation Letters* (2022).

[8] Y. Zhang, X. Liang, D. Li, S. S. Ge, B. Gao, H. Chen, T. H. Lee, Barrier lyapunov function-based safe reinforcement learning for autonomous vehicles with optimized backstepping, *IEEE Transactions on Neural Networks and Learning Systems* 35 (2) (2022) 2066–2080.

[9] M. Jabari, A. Botta, L. Tagliavini, C. Visconte, G. Quaglia, A safe, high-precision reinforcement learning-based optimal control of surgical continuum robots: A monotone tube boundary approach with prescribed-time control capability, *Robotics and Autonomous Systems* 190 (2025) 104992.

[10] Y. Chow, O. Nachum, E. Duenez-Guzman, M. Ghavamzadeh, A lyapunov-based approach to safe reinforcement learning, *Advances in neural information processing systems* 31 (2018).

[11] L. Zhao, K. Gatsis, A. Papachristodoulou, Stable and safe reinforcement learning via a barrier-lyapunov actor-critic approach, in: 2023 62nd IEEE Conference on Decision and Control (CDC), IEEE, 2023, pp. 1320–1325.

[12] K. Li, Z. Olkin, Y. Yue, A. D. Ames, Clf-rl: Control lyapunov function guided reinforcement learning, arXiv preprint arXiv:2508.09354 (2025).

[13] A. Anand, K. Seel, V. Gjærum, A. Håkansson, H. Robinson, A. Saad, Safe learning for control using control lyapunov functions and control barrier functions: A review, *Procedia Computer Science* 192 (2021) 3987–3997.

[14] M. H. Shahna, J. Mattila, Synthesis of deep neural networks with safe robust adaptive control for reliable operation of wheeled mobile robots, arXiv preprint arXiv:2508.10634 (2025).

[15] D. Martinez-Baselga, L. Riazuelo, L. Montano, Rumor: Reinforcement learning for understanding a model of the real world for navigation in dynamic environments, *Robotics and Autonomous Systems* (2025) 105020.

[16] A. Alexander, V. S. Vangaveeti, K. Venkatesan, J. Mounsef, K. Ramanujam, Adaptive emergency response and dynamic crowd navigation for mobile robot using deep reinforcement learning, *Frontiers in Robotics and AI* 12 (2025) 1612392.

[17] P. Osinenko, G. Yaremenko, R. Zashchitin, A. Bolychev, S. Ibrahim, D. Dobriborsci, Critic as lyapunov function (calf): a model-free, stability-ensuring agent, in: 2024 IEEE 63rd Conference on Decision and Control (CDC), IEEE, 2024, pp. 2517–2524.

[18] M. H. Shahna, P. Mustalahti, J. Mattila, Robust torque-observed control with safe input–output constraints for hydraulic in-wheel drive systems in mobile robots, *Control Engineering Practice* 164 (2025) 106459.

[19] P. Osinenko, D. Dobriborsci, W. Aumer, Reinforcement learning with guarantees: a review, *IFAC-PapersOnLine* 55 (15) (2022) 123–128.

[20] G. Yaremenko, D. Dobriborsci, R. Zashchitin, R. C. Maestre, N. Q. H. Hoang, P. Osinenko, A novel agent with formal goal-reaching guarantees: an experimental study with a mobile robot, arXiv preprint arXiv:2409.14867 (2024).

[21] C. Campos, R. Elvira, J. J. G. Rodríguez, J. M. Montiel, J. D. Tardós, Orb-slam3: An accurate open-source library for visual, visual–inertial, and multimap slam, *IEEE transactions on robotics* 37 (6) (2021) 1874–1890.

[22] M. H. Shahna, P. Mustalahti, J. Mattila, Nmpc-augmented visual navigation and safe learning control for large-scale mobile robots, arXiv preprint arXiv:2601.00609 (2026).

[23] M. H. Shahna, E. Haaparanta, P. Mustalahti, J. Mattila, Lidar-inertial slam-based navigation and safety-oriented ai-driven control system for skid-steer robots, in: 2025 IEEE 64th Conference on Decision and Control (CDC), 2025, pp. 7795–7802.



Mehdi Heydari Shahna received the B.Sc. degree in Electrical Engineering from Razi University, Iran, in 2015, the M.Sc. degree in Control Engineering from Shahid Beheshti University, Iran, in 2018, and the D.Sc. (Tech.) degree in Automation Science and Engineering from Tampere University, Finland, in 2025. He is currently a postdoctoral researcher at Tampere University. His research interests include robot learning, safe control, robust control, and nonlinear systems.



Seyed Adel Alizadeh Kolagar received his M.Sc. degree in Mechanical Engineering from Sharif University of Technology. He is currently a Ph.D. student in Automation Science and Engineering. His research interests include robot learning, reinforcement and imitation learning, robotics, and machine learning.



Jouni Mattila received an M.Sc. and Ph.D. in automation engineering from Tampere University of Technology, Tampere, Finland, in 1995 and 2000, respectively. He is currently a professor of machine automation in the Automation Technology and Mechanical Engineering Unit at Tampere University. His research interests include machine automation, nonlinear-model-based control of robotic manipulators, and energy-efficient control of heavy-duty mobile manipulators.